3D DEFORMATION MEASUREMENT OF CONCRETE WALL USING CLOSE-RANGE PHOTOGRAMMETRY

Tee-Ann Teo [a] [*]

[a] Dept. of Civil Engineering, National Chiao Tung University, Hsinchu, Taiwan 30010 - tateo@mail.nctu.edu.tw

Commission II, WG II/10

ABSTRACT:

Due to the development of digital image processing, digital photogrammetry is becoming an interesting research area in the field of structural monitoring in civil engineering. This study presents a photogrammetric measurement technique for concrete wall deformation monitoring in the destructive experiment. The non-contact photogrammetric measurement technique which provides surface deformation, is more flexible than the contacted single-point measurement technique (e.g., linear variable displacement transducers, LVDT). The major steps of the proposed scheme include (1) camera calibration, (2) orientation modeling, (3) 3D dense matching, and (4) filtering and interpolation for surface deformation. This experiment used two non-metric digital cameras to measure the deformation of a concrete wall in destructive experiment. The validation compared the image-derived and ranger-derived displacements during the experiment with mean error and standard errors of 32 epochs were -0.02mm and 0.81mm, respectively. The correlation between image-derived displacement and LVDT-derived displacement was 0.9803. The advantage of photogrammetry is to derive surface deformation which covered the whole wall during the experiment. In summary, this study demonstrated that photogrammetry is a useful measurement technique for concrete wall destructive experiment.

1. INTRODUCTION

In traditional destructive experiment for concrete structures, the displacement of concrete structures caused by external forces is usually measured by the contact instrument such as dial gauges and linear variable displacement transducers (LVDTs). Although this type of instrument can accurately measure the displacement inside its linear range, a single instrument can only measure the displacement of a single point, so more LVDT instruments are needed to obtain more measurement points. And the another concern is the LVDT instrument might be damaged while the concrete is close to failure.

Instead of using the contact instrument, photogrammetry (Fraser and Riedel, 2000) or laser scanning (Gordon et al., 2003) adopts the non-contact technique to measure the object displacements. The photogrammetric measurement is based on angle measurement, while the laser scanning is based on range measurement. Considering the imaging device is more cost-effective than the laser unit, this study adopts the photogrammetric measurement technique in destructive experiment.

Several studies demonstrated the applications of photogrammetry measurement for different types of structural elements, for example, concrete beams (Whiteman et al., 2002), steel beams (Fraser and Riedel, 2000), and bridge (Jiang et al., 2008). Whiteman et al. (2002) used the photogrammetry method to measure the deflection of concrete beams. The experimental configuration was to place some target points on the concrete beam surface, some fixed target points in front and behind the concrete beam, and two cameras were used to capture images during the experiment on different loadings. The experimental results showed that the displacement of concrete beams measured by close-range photogrammetry achieved sub-millimeter

accuracy, which is roughly consistent with the data recorded by LVDT. Lee and Al-Mahaidi (2008) studied the shear force changes in reinforced concrete T-beams with CFRP (carbon fiber reinforced polymer) using close-range photogrammetry. The purpose is to determine the shear deformation mechanism of T-beams. This study showed that photogrammetry may derive different useful parameters such as crack width, shear behavior, and average strain. The experiment compared the results between photogrammetry and traditional measuring instruments. The photogrammetry technology is more efficient and preserves acceptable accuracy with minimum preparation.

Valença et al., (2012) applied the photogrammetry technique to monitor the structural behavior of long-span beams and large structures (i.e., bridge), the study concluded that photogrammetry is useful for structural monitoring. The advantages of photogrammetry technique are: (1) to obtain unlimited measuring points using automatic image processing; (2) the data acquisition (or imaging) is much more flexible than traditional methods. The photogrammetry can also be applied to the crack detection for structural monitoring. For example, Liebold & Maas (2016) used spatio-temporal filtering techniques to reduce noise effects in photogrammetric crack monitoring. The proposed method detected crack from the image sequences of the concrete beam under varying load conditions. Thus, the close-range photogrammetry technique becomes an important tool for structural monitoring in civil engineering.

Many studies in the literature use close-range photogrammetry to measure deflection and displacement for concrete and steel beams in the 1D vertical direction or 2D displacement fields. The 3D deformation in structural monitoring is usually implemented by the laser scanner (González-Aguilera et al., 2008). As this study is focusing on the concrete wall, the behavior of surface deformation is the major concern in the destructive experiment.

---

* Corresponding author.

Therefore, the objective of this research is to performing the 3D deformation measurement for the concrete walls using photogrammetry techniques. The 3D surface deformation of the concrete wall under varying load conditions will be derived by photogrammetric measurement technique.

2. INSTRUMENTATIONS

This study measures the deformation of a 2m by 2m concrete brick wall. Ten cardboards for orientation modeling are pasted on the wall. Besides, 99 (9 rows x 11 cols) circle target points are painted for deformation monitoring. The average distance between circle target points is about 15cm. Two cameras and one LVDT are fixed on tripods in front of the concrete wall. And an additional fixed ranger is used to measure the distance between ranger and wall during the whole experiment, to support when the LVDT is removed at concrete is close to failure. Figure 1 shows the configuration of the deformation experiment.
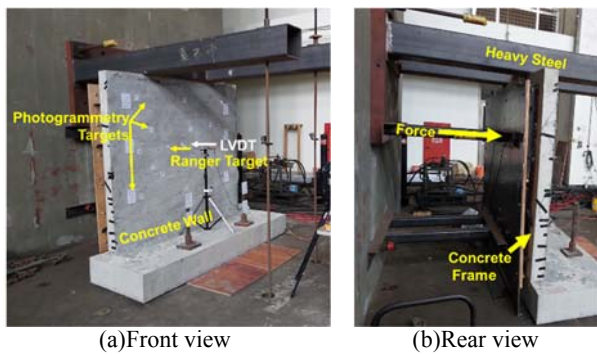

(a)Front view   (b)Rear view
Figure 1. Concrete wall

2.1 Cameras

Two non-metric fixed lens cameras (i.e., Sony A65 and Nikon D850) were used in the experiments. The focal lengths of the fixed camera lens are 30mm and 28mm, respectively. The resolutions for Sony A65 and Nikon D850 were 6000 x 3376 pixels and 8256 x 5504 pixels, respectively. These two cameras are fixed on tripods and synchronize by an IR remote controller.

2.2 LVDT and Ranger

This study uses an LVDT with 0.5% linearity error to measure the displacement at the wall center. The measurement range of this RDP DCTH2000 displacement transducer is within 50mm, and the sampling frequency for the data logger is set up at 20hz. Because the LVDT will remove when the concrete wall is near to failure, this study uses an additional ranger to evaluate the displacement derived from photogrammetry. The ranger is Leica DISTO D810 with 1.0 mm accuracy. This ranger is fixed on a tripod during the experiment, and controlled by a notebook via bluetooth interface. There is no need to touch the ranger when recording the range measurement. Besides, a signalized sticker for the laser is also pasted on the concrete wall to have a better return signal.

3. EXPERIMENTS AND RESULTS

The proposed scheme includes four major parts: (1) camera calibration, (2) orientation modeling, (3) 3D dense matching, and (4) filtering and interpolation for surface deformation. The camera calibration determines the interior parameters of the camera before data acquisition. The calibrated cameras take the sequence images for the concrete wall in different loadings. The bundle adjustment technique is utilized to obtain the exterior

orientations. Then, semi-global matching (SGM) algorithm is adopted to obtain dense 3D point clouds (Remondino et al., 2014). Finally, the non-surface points are filtered and only the surface points are interpolated to generate the 3D wall surface. The sequence of 3D wall surfaces represents the deformation of concrete wall under different loadings. The details of the experiment and results are provided in the following sections.

3.1 Camera Calibration

The camera calibration for the non-metric fixed-lens camera is performed just before the concrete wall experiments. This study uses the Brown distortion model (equations (1) to (4)) (Brown, 1971) to determine the lens distortion (Teo, 2015). A commercial software iWitness is used to calibrate the camera, the iWitness uses circular signalized targets and self-calibration to determine the lens distortion parameters (Fraser and Hanley, 2004). The calibrated parameters are shown in Table 1.

$$\Delta x = \Delta x_r + \Delta x_d$$
$$\Delta y = \Delta y_r + \Delta y_d \tag{1}$$

$$\Delta x_r = \bar{x} \times (K_1 r^2 + K_2 r^4 + K_3 r^6)$$
$$\Delta y_r = \bar{y} \times (K_1 r^2 + K_2 r^4 + K_3 r^6) \tag{2}$$

$$\Delta x_d = P_1(r^2 + 2\bar{x}) + 2P_2 \overline{xy}$$
$$\Delta y_d = P_2(r^2 + 2\bar{y}) + 2P_1 \overline{xy} \tag{3}$$

$$r = \sqrt{(\bar{x})^2 + (\bar{y})^2} = \sqrt{(x - x_0)^2 + (y - y_0)^2} \tag{4}$$

Where, (Δx, Δy) are total lens distortion; (Δx_r, Δy_r) are radial distortion; (Δx_d, Δy_d) are tangential distortion; (K_1~K_3) are coefficients of radial distortion; (P_1~P_2) are coefficients of tangential distortion; r is radial distance; (x,y) are photo coordinate; and (x_0, y_0) are principal points.

	Sony A65	Nikon D850
Image size(pixel)	6000 x 3376	8256 x 5504
Pixel size(um)	3.889	4.4345
Focal length(mm)	30.925874	29.061846
xp (mm)	0.098727	0.000722
yp (mm)	0.147963	-0.000095
k1	1.2649e-04	9.2251e-05
k2	-1.1435e-07	-7.2513e-08
k3	-2.2086e-10	-4.1891e-11
p1	-1.6251e-05	9.5623e-06
p2	-6.6231e-05	2.3245e-05
Estimated internal accuracy (pixel)	0.25	0.29

Table 1. Camera parameters

3.2 Orientation Modeling

During the experiment, two cameras are fixed on tripods in front of the concrete wall, as figure 2 shown images from these two cameras. The distances from the wall to cameras are about 3m, and the spatial resolution is better than 0.5mm on the concrete wall. Besides, the convergence angle for stereo images is 42 degrees. The convergent angle means the intersection angle between two light rays to the wall center. This study assumed that these two cameras are fixed and only the concrete wall is a moving object. The orientation modeling aims to calculate the exterior camera parameters (i.e., camera poses and camera viewing angles) before the experiment. This study uses the

iWitness card board to obtain relative orientation between cameras automatically. Then, four control points on the concrete wall are manually measured to obtain the absolute orientation via bundle adjustment (Fraser and Hanley, 2004). The number of tie points is 56 points, while the number of control points is 4 points. The root-mean-squares error of bundle adjustment in image space is 0.54 pixels. The results of bundle adjustment are shown in Table 2.
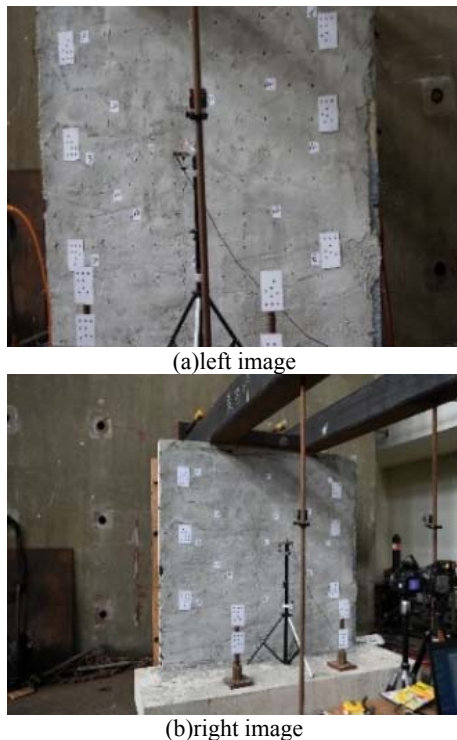

(a)left image

(b)right image
Figure 2. Images from two cameras

	Sony A65	Nikon D850
Xc(m)	1.563	-1.011
Yc(m)	-0.208	-0.199
Zc(m)	3.385	3.203
Omega(Deg)	-2.101	-0.964
Phi(Deg)	13.650	-20.328
Kappa(Deg)	-1.890	-0.275

Table 2. Exterior orientation parameters

3.3 3D Dense Matching

After the orientation modeling, a semi-global matching (SGM) (Remondino et al., 2014) algorithm is applied to obtain 3D point clouds from stereo images. The idea of SGM is to determine the semi-global minimum energy in the epipolar image space. The SGM is a robust stereo matching algorithm to extract dense points from stereo images. As the cameras are all fixed on the tripods, the time series stereo images use the same orientation parameters. A commercial software SURE (Rothermel et al., 2012) is used to obtain time-series point clouds from time series stereo images. Figure 3 shows an example of 3D dense points. The point density near to the center part is higher than the concrete boundary. The overall average point density is 729 points per square centimeter. The overall average point spacing is about 3mm in the non-occlusion region. The occussion is caused by the tripod of LVDT and the poles between the camera and concrere wall.
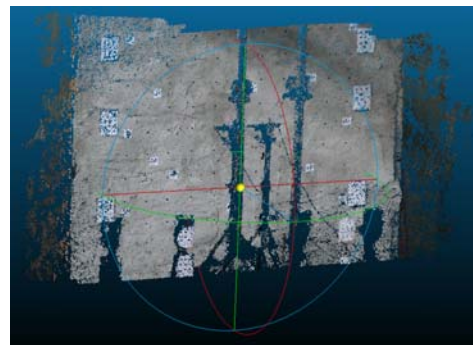

Figure 3. All 3D point clouds from stereo images

3.4 Filtering and interpolation

The dense matching stage extracts both 3D wall points and 3D non-wall points simultaneously. As the experiment is focused on the 3D deformation of the concrete wall, the 3D non-wall points have to be filtered before analysis. This study assumes that the concrete wall is a planar object. Therefore, an iterative plane fitting process is applied to remove the non-wall points. This plane fitting process iteratively removes non-wall points when the point-to-plane distances are larger than 2.5 sigmas. After non-wall point are filtered, the remaining data are irregular points.

To obtain the 3D deformation of the wall, the regular grided wall points are needed to form the surface deformation. This study applies triangulated irregular network (TIN) interpolation to obtain gridded wall points. Figures 4a and 4b show an example of wall points after filtering and triangulated mesh.
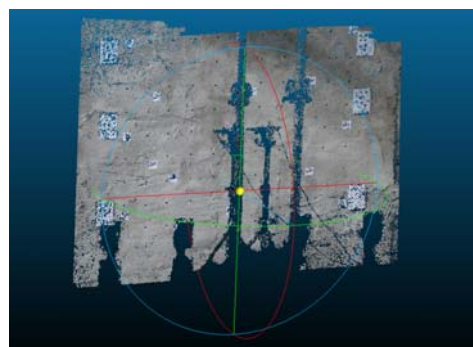
(a) Wall point only
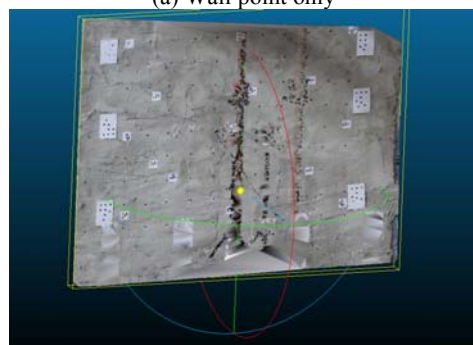
(b) Grided wall
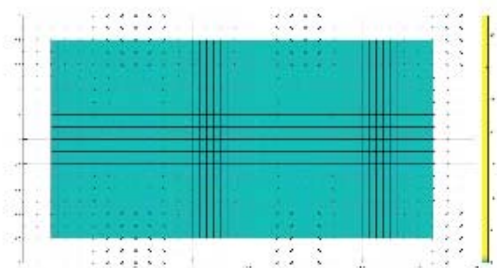Figure 4. Filtering and interpolation

4. PRELIMINARY ANALYSIS

The analysis includes the following stages: (1) results of 3D Wall deformation; (2) comparison of image-derived and ranger-derived displacements; (3) correlation of image-derived and LVDT-derived displacements. The details of data analysis is provided in the following sections.

4.1 3D deformation measurement for concrete wall

The duration of adding the external force to the concrete wall was 105 minutes. The total number of stereo images is 36 pairs during the experiment. The first pair was taken before the experiment and the wall is not moving at this pair. All the other stereo pairs were referring to the first pair and extracting the displacement by comparing the first epoch and current epoch. Figure 5 shows the results of 3D deformation at epochs 1 (time=0sec), 16 (time=1800sec) and 29 (time=1940sec). Different colors indicate different displacements and the yellow color show higher displacement than blue color. In this study, the spacing of the grid is 2.5cm, which means every 2.5cm x 2.5cm has a 3D displacement.

The wall is not moving in the first epoch. Therefore the figure 5a show uniform color. In the middle of experiment (i.e. epochs 16), the upper left area show larger displacement than upper right (figure 5b). When the concrete wall is near to failure (i.e. epochs 29), the upper region shows higher displacement than the lower part (figure 5c). The results show that, the photogrammetry technique is able to provide 3D displacement for concrete wall. Although the concrete is partially occluded by the tripod of LVDT, the interpolation may recover the 3D surface as we assume the displacements were uniform during the experiment.

(a) Wall deformation at epoch 01
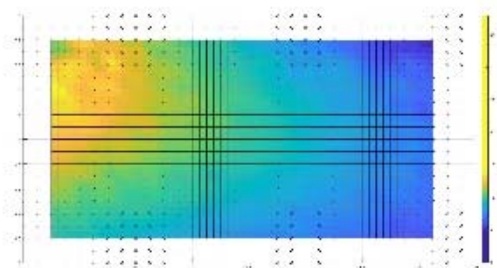
(b) Wall deformation at epoch 16
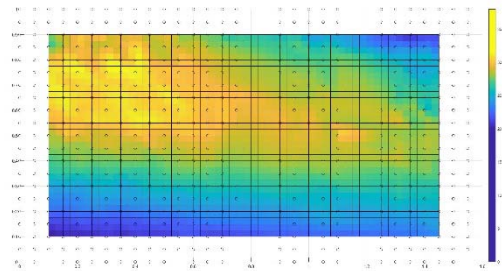
(c) Wall deformation at epoch 29
Figure 5. Filtering and interpolation

4.2 2D Profile analysis

The other way to understand the behaviour of concrete wall during experiment is 2D profile analysis. The displacement of wall and also the deformation of wall can be analysed by 2D profile analysis. Figure 6 show an example of 2D vertical profile on the right side of concrete wall. The Y-axis is vertical direction while X-axis is the delta Z opposite wall surface. Each line represent the cross-section of wall in vertical direction in different epochs (i.e., epochs 1, 16 and 29). The distance between two vertices in vertical direction (i.e., Y-axis) is about 10cm. The 2D profile indicates the displacement and deformation of wall in different stages. When external force is continuously applied to the wall, the wall slanted towards force direction and also have deformation in the upper part.
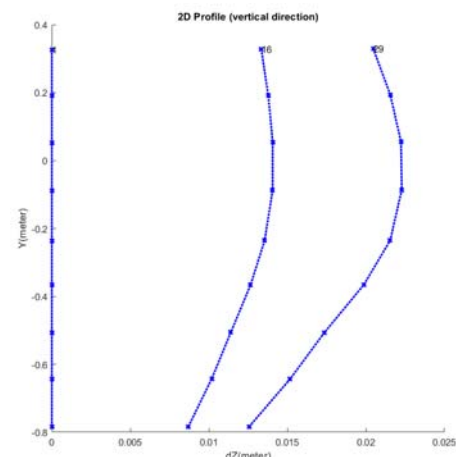

Figure 6. Profile analysis.

4.3 Comparison of image-derived and ranger-derived displacements

In order to evaluate the accuracy of image-derived displacement, the image-derived 3D points near to the ranger's observation were selected for accuracy analysis. The ranger can only measure a single location while photogrammetry is able to measure many 3D points over a region. Therefore, this study used the mean value within 10mm by 10mm to represent the image-derived displacement. The mean error and standard errors of 32 epochs were -0.02mm and 0.81mm, respectively. Figure 7 compares image-derived and laser-derived displacements. The image-derived displacement shows higher consistency with laser ranger.
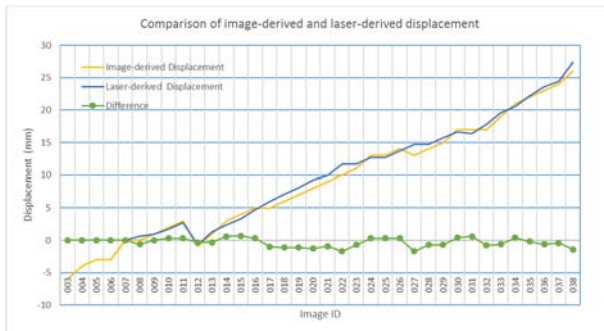
Figure 7. Comparison of image-derived and laser-derived displacements.

4.4 Comparison of image-derived and LVDT-derived displacements

For safety reason, the LVDT were removed at the epoch 21. There is only 21 datasets can be used in the comparison of image-derived and LVDT-derived displacements. Because the LVDT and ranger have a linearity error, this session used R-square to exanimate the correlation between image-derived and LVDT-derived displacements. For these 21 points, the correlation between image-derived displacement and LVDT-derived displacement was 0.9803. Figure 8 compares image-derived and LVDT-derived displacements. The image-derived displacement also shows a higher correlation with LVDT-derived displacement.
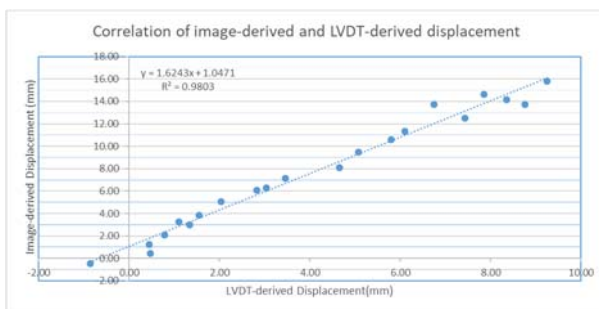

Figure 8. Correlation of image-derived and LVDT-derived displacements.

5. CONCLUSIONS AND FUTURE WORKS

This study proposed a non-contact photogrammetry scheme to obtain 3D deformation for concrete wall destructive experiments. The major works were orientation modeling, 3D dense matching, and non-wall point filtering. The experiment used two non-metric digital cameras to measure the deformation of a concrete wall. The extracted sequence 3D wall surfaces represent the deformation of a concrete wall under different loadings. The validation compared the image-derived and ranger-derived displacements during the experiment. The mean error and standard errors of 32 epochs were -0.02mm and 0.81mm, respectively. The correlation between image-derived displacement and LVDT-derived displacement was 0.9803. The experiment demonstrated that photogrammetry is a useful measurement technique for concrete wall destructive experiment. Future work will focus on reducing the noise and improving the positioning accuracy of 3D points. Besides, there were some hidden areas from two view points. Future work will set up more cameras to have multi-view images for the reduction of the hidden area.

REFERENCES

Brown, D. C. 1971. Close-range camera calibration, Photogrammetric Engineering. Engineering and Remote Sensing, 37(8), 855-866.

Fraser, C. S., & Hanley, H. B. 2004. Developments in close-range photogrammetry for 3D modelling: the iWitness example. In Presented paper, International Workshop: Processing and Visualization using High-Resolution Imagery, Pitsanulok.

Fraser, C. S., & Riedel, B. 2000. Monitoring the thermal deformation of steel beams via vision metrology. ISPRS Journal of Photogrammetry and Remote Sensing, 55(4), 268-276.

González-Aguilera, D., Gómez-Lahoz, J., & Sánchez, J. 2008. A new approach for structural monitoring of large dams with a three-dimensional laser scanner. Sensors, 8(9), 5866-5883.

Gordon, S. J., Lichti, D., Stewart, M., & Franke, J. 2003. Structural deformation measurement using terrestrial laser scanners. Proceedings of 11th FIG Symposium on Deformation Measurements, Santorini, Greece.

Jiang, R., Jáuregui, D. V., & White, K. R. 2008. Close-range photogrammetry applications in bridge measurement: Literature review. Measurement, 41(8), 823-834.

Liebold, F., & Maas, H. G. 2016. Advanced spatio-temporal filtering techniques for photogrammetric image sequence analysis in civil engineering material testing. ISPRS Journal of Photogrammetry and Remote Sensing, 111, 13-21.

Remondino, F., Spera, M. G., Nocerino, E., Menna, F., & Nex, F. 2014. State of the art in high density image matching. The photogrammetric record, 29(146), 144-166.

Rothermel, M., Wenzel, K., Fritsch, D., & Haala, N. 2012. SURE: Photogrammetric surface reconstruction from imagery. Proceedings LC3D Workshop, Berlin. 8(2): 2012.

Teo, T. 2015. Video-based point cloud generation using multiple action cameras. The International Archives of Photogrammetry, Remote Sensing and Spatial Information Sciences, 40(4), 55.

Valença, J., Júlio, E. N. B. S., & Araújo, H. J. 2012. Applications of photogrammetry to structural assessment. Experimental Techniques, 36(5), 71-81.

Wahbeh, A. M., Caffrey, J. P., & Masri, S. F. 2003. A vision-based approach for the direct measurement of displacements in vibrating systems. Smart materials and structures, 12(5), 785.

Whiteman, T., Lichti, D. D. & Chandler, I. 2002. Measurement of deflections in concrete beams by close-range digital photogrammetry, Geospatial Theory, Processing and Applications, 34(4):40-48.